VALIDITY OF SMALL SCALE TESTS FOR TURRET/FAIRING LOADS AND CAVITY EFFECTS

BY

Daniel J. McDermott
James T. Van Kuren

Aeromechanics Division
Air Force Flight Dynamics Laboratory
Wright-Patterson Air Force Base, Ohio 45433

ABSTRACT

Numerous wind tunnel tests have been conducted by the Air Force and NASA to investigate the aerodynamic/airframe integration of an airborne optical pointing and tracking system. A common feature of the various systems tested is the use of a fuselage mounted open-port turret to house the optics. The suppression of undesirable aerodynamic phenomena within the open port cavity together with the development of aerodynamic fairings for the reduction of base pressure drag behind the turret has received special attention. In this paper, data from several wind tunnel experiments along with available flight test data are used to discuss the validity of these small scale tests and their inherent limitations. Tests were performed at transonic speeds to measure the turbulence levels in a cavity with and without a forward porous fence, turret drag with and without an aerodynamic fairing, and turret/fairing unsteady pressures.

LIST OF SYMBOLS

A_T	Turret Forward Projected Area
d	Cavity Width
D	Turret Diameter
f	Frequency, Hz
F	Friction force
h	Fence Height
Hz	Hertz, One Cycle per Second
k	Ratio of Specific Heats
kHz	Kilohertz = 1000 Hz
ℓ	Distance from Plate Leading Edge or Characteristic Length
m	Integer That Defines Mode Number
M	Mach Number
P	Pressure Force
P_{rms}	Root Mean Square Pressure
q	Free Stream Dynamic Pressure
R_D	Reynolds Number Based on Turret Diameter D
$R_D(M)$	Reynolds Number Based on Turret Diameter D as a Function of Mach Number M
R_ℓ	Reynolds Number Based on Distance ℓ
S	Strouhal Number = fd/V_∞ or fD/V_∞
u	Velocity Anywhere in the Boundary Layer in the x Direction
V_∞	Free Stream Velocity
x	Distance Along the Model Centerline in the Free Stream Direction. Measured from Plate or Cavity Leading Edge
y	Distance From the Model Centerline Normal to the Free Stream

LIST OF SYMBOLS (CONT'D)

δ	Boundary Layer Disturbance Thickness
δ_1	Boundary Layer Displacement Thickness
δ_2	Boundary Layer Momentum Thickness
$\delta_\ell(x)$	Laminar Boundary Layer Disturbance Thickness as a Function of x
$\delta_t(x)$	Turbulent Boundary Layer Disturbance Thickness as a Function of x
ΔC_D	Incremental Drag Coefficient = $\frac{\text{Drag Force}}{\frac{1}{2}\rho_\infty V_\infty^2 \; A_T}$
ε_t	Turbulent Momentum Eddy Diffusivity
μ	Dynamic Viscosity
ρ	Mass Density Anywhere in the Boundary Layer
ρ_∞	Free Stream Mass Density
τ_ℓ	Laminar Shear Stress
τ_t	Turbulent Shear Stress
Φ	Power Spectral Density of Pressure, $\left[\frac{\text{Force}}{\text{Length}^2}\right]^2/\text{Hz}$

SECTION I

INTRODUCTION

BACKGROUND

During the past ten years the Air Force and NASA have conducted numerous wind tunnel tests to investigate the aerodynamic/airframe integration of an airborne optical pointing and tracking system. A common feature of the various systems tested has been the use of a fuselage mounted turret to house the optics. The light beam propagates from the optical platform through an open port in the turret and thus eliminates the losses associated with a solid material window. However, the optical beam quality and the performance of the pointing and tracking system are still very much a function of the external aerodynamic flow field. When exposed to the free stream flow the open port turret acts as a cavity, and under a resonance condition, internal unsteady pressure fluctuations become significant. These acoustical resonances create unwanted vibrations of the internal optical components and thus degrade the overall system performance. In addition, flow separation on the turret creates unsteady external torques while increasing the total aircraft drag.

In the above mentioned wind tunnel tests, the suppression of undesirable aerodynamic phenomena within these cavities together with the development of aerodynamic fairings for the reduction of base pressure drag behind the turret, has received special attention (References 1,2,3,4,5,6). Since much time has been spent in these developmental areas a data comparison of various scale wind tunnel tests is desirable. In this paper, data from several of the wind tunnel experiments along with available

flight test data are used to discuss the validity of these small scale tests and their inherent limitations.

SECTION II

FLUID FLOW CONCEPTS

Before discussing the wind tunnel results it's worthwhile to recall a few concepts governing different flow processes which have a direct affect on the comparison of large and small scale test data. The understanding of these concepts points out some inherent limitations of small scale tests and helps in the interpretation of such data.

REYNOLDS NUMBER AND DYNAMIC SIMILARITY

Approximately 100 years ago Osborne Reynolds identified the importance of the ratio of inertial to viscous forces in defining the character of fluid flows in pipes, i.e., whether the flow will be laminar or turbulent. The introduction of this ratio, $\rho_\infty V_\infty \ell/\mu$, referred to as the Reynolds number, contributed significantly to another important concept call Dynamic Similarity. Consider an experiment where a low speed fluid flows around two geometrically similar bodies. If the flow properties are measured at geometrically similar locations, and their respective Reynolds numbers are identical, then the two experiments are said to be dynamically similar. In others words, two flow systems are said to be dynamically similar if they are geometrically similar and the forces in one system are in the same ratio to each other as the forces in the second system. The practical importance of the principle of similarity is that inexpensive wind tunnel tests of scale models can be used to predict the performance of full-scale aircraft. However, in many instances several force ratios are involved and consequently it is

impossible to have complete dynamic similarity. For example, when measuring drag on an airfoil in high speed flow both compressible gas forces and viscous shear forces are important. In general, complete similarity in such cases is possible only for full scale models.

BOUNDARY LAYER CONCEPT

Since the Reynolds number is the ratio of the inertial forces to viscous forces one might expect that viscous forces would be negligible at very high Reynolds numbers. The fact is, that no matter how large the Reynolds number, viscous forces can never be completely ignored. The reason for this is that fluid particles do not slip at the surface of a solid boundary. Thus, the imposed boundary condition is that the tangential velocity at the wall is zero. Moving outward from the wall the velocity increases to a value nearly equal to that of the free stream. This region of retarded flow is called the "boundary layer".

The development of a boundary layer can best be illustrated by a study of an incompressible, uniform flow over a flat plate (see Figure 1). As the fluid particles reach the plate leading edge, large shear stresses are created at the surface which slows down the fluid. This relatively thin region close to the body surface varies in "thickness" downstream along the plate. The actual boundary layer thickness δ is usually defined as the distance from the surface to the point where the local velocity u equals ninety-nine percent of the free stream velocity V_∞. Since the term boundary layer thickness is somewhat ambiguously defined, more useful terms such as displacement thickness δ_1 and momentum thickness δ_2 are often used. The displacement thickness δ_1 is a measure of the displacement of the free stream flow away from the plate and is defined as:

$$\delta_1 = \int_0^\infty \left[1 - \frac{\rho u}{\rho_\infty V_\infty}\right] dy$$

where ρ and ρ_∞ are the local and free stream mass densities respectively. The momentum thickness δ_2 is a measure of the deficit of momentum flux caused by the boundary layer and is proportional to the drag on the plate. The momentum thickness δ_2 is defined as:

$$\delta_2 = \int_\phi^\infty \frac{\rho u}{\rho_\infty V_\infty}\left[1 - \frac{u}{V_\infty}\right] dy$$

The boundary layer along the plate is separated into a laminar, transitional and turbulent region. Depending mostly on the local Reynolds number the boundary layer remains laminar for some distance along the plate. In this region the viscous shear stress τ_ℓ is proportional to the velocity gradient, that is:

$$\tau_\ell \sim \frac{du}{dy}$$

In laminar flow the transport of momentum is molecular in nature. The transport coefficient is called the dynamic viscosity μ and is a function only of the fluid properties. Thus the laminar shear stress can be expressed as:

$$\tau_\ell = \mu \frac{du}{dy}$$

The layer remains truly laminar up to the transition point but after this "critical point" (more usually defined by a "critical Reynolds

number") small disturbances or fluctuations are amplified in magnitude, eventually becoming so large as to disrupt the laminar flow pattern which then breaks up into large eddies. Such disturbances are introduced from the free stream or by surface irregularities, both of which are always present to some degree. Once the turbulent mixing process starts, some distance is required for an equilibrium mixing process to be established. Hence, transition requires a "zone" rather than suddenly occurring at a point. Thereafter, the characteristics of the layer are essentially turbulent in nature.

In turbulent flow the transport of momentum is greatly enhanced. Consequently the shear stress is higher than in the laminar flow case (see Figure 1). Expressions for the viscous shear stress have been developed which are similar to the laminar equation. However, the turbulent momentum transport coefficient is by no means a constant but rather a function of the dynamics of the flow. This turbulent coefficient, ε_t, is both a function of the magnitude of the velocity fluctuations and eddy scale size. Thus the turbulent shear stress can be expressed as:

$$\tau_t = \varepsilon_t \frac{du}{dy}$$

The above description of a boundary layer has indeed been a simplified one. Many aspects of boundary layers such as effects of compressibility, pressure gradient, wall shape and wall temperature were not addressed. However, it is found that drag due to viscous shear stresses is higher when the flow is completely turbulent.

DRAG FORCES FOR BLUNT AND STREAMLINED BODIES

Newton's law of motion states, that for a constant mass, the sum of the external forces on a body is equal to the product of its mass and acceleration. In fluid aerodynamics,the two surface forces which are of particular importance are friction forces and pressure forces. The relative importance of these two forces play a significant role in the drag of blunt and streamlined bodies such as a fuselage mounted turret/ fairing (see Figure 2). As was previously discussed, the magnitude of the viscous drag depends on whether the surface boundary layer is laminar or turbulent. For high Reynolds number flows the boundary layer is mostly turbulent and the viscous drag is higher than for low Reynolds number flows where the boundary layer is laminar. Therefore, it is important to maintain a laminar boundary layer on a streamlined body where the pressure drag is small. In contrast, and for a different reason, turbulent flow is also of importance on a blunt shaped body. When a fluid flows around a blunt body,the boundary layer starts out laminar and tends to separate from the surface creating a low pressure wake. This low pressure region acts as a drag force on the body and its magnitude is a function of the location on the body where the flow separates. For such cases, early transition from laminar to turbulent flow would have the effect of reducing the size of the wake and thus reducing the pressure drag. Drag reduction of this form is therefore very much a function of Reynolds number. Recall that transition can also be a function of free stream turbulence and surface roughness. A high free stream turbulence could cause earlier transition which would help reduce the pressure drag. Surface roughness could also cause a drag reduction but is very dependent on Reynolds number.

WIND TUNNEL TESTING

The wind tunnel is probably the aeronautical engineer's most important design and development tool. Excellent agreement between small and full scale tests can be obtained when the various force systems involved are properly modeled. Indeed, proper modeling is implied by the principles of similarity discussed earlier. Generally speaking this statement is true. However, it's true only if *all* the pertinent parameters are the same. For example, the drag force on a blunt body could be a function of Mach number, Reynolds number, geometry, and free stream turbulence. Matching the Mach number, Reynolds number and geometry may not be sufficient. Since boundary layer transition and separation are affected by the free stream turbulence level, the drag force measured in two different wind tunnel tests may not be the same. In addition, local steady and unsteady pressure measurements can be significantly influenced by the degree of free stream turbulence, the location of transition and local separated flow regions. Spatial resolution of local instrumentation on a small scale model should also be considered. The measurement may really be an integrated effect over a relatively large surface area!

All things considered, the wind tunnel testing of small scale models has proven very useful to the aeronautical engineer. The principles of dynamic similarity and an understanding of the basic fluid flow concepts help the engineer to interpret such data. When dynamic similarity is incomplete the data trends are still very important results. Much of the data presented in this paper shows good correlation between tests. Some of the anomalies that are present can be attributed to one or more of the reasons discussed in this section.

SECTION III

CAVITY AND FENCE TESTS

MODELS AND TEST FACILITIES

Two separate models of a 15.2 cm (6 in.) cube shaped cavity mounted on a flat plate were tested in the Air Force Flight Dynamics (AFFDL) 0.61 m by 0.61 m (2 ft by 2 ft) and NASA-Ames 1.83 m by 1.83 m (6 ft by 6 ft) transonic wind tunnels. The dimensions of these two models are shown in Figures 3a and 3b. Several porous fences which were designed to reduce the turbulence levels in the cavity could be mounted upstream of the cavity in one of three different locations. The results from two of these fence configurations are presented in this paper. Their dimensions and location upstream of the cavity are given in Table 1.

The NASA-Ames flat plate model was mounted in the tunnel on a center pylon sufficiently far from the wall to assure that the plate was not immersed in the tunnel boundary layer (Ref. 7). An elliptic leading edge of major axis four times the minor axis was used to preclude separation and to reduce the mass flow and blockage beneath the plate. The AFFDL flat plate model was mounted on the side wall of the 0.38 m by 0.38 m (1.25 ft by 1.25 ft) transonic test section. This particular test section has slotted walls and a removable section sidewall which protrudes 3.81 cm (1.5 in.) into the flow, thus bleeding off the boundary layer.

TYPES OF MEASUREMENTS AND TEST CONDITIONS

Data recorded during the cavity tests included both mean and unsteady pressure measurements. Dynamic pressure transducers were located at key

positions inside the cavity and on the flat plate forward and aft of the cavity. Total pressure probes were also used to measure the velocity profiles at the leading edge of the cavity with and without a porous fence. Only a portion of the unsteady pressure measurements are presented in this paper. The discussion is limited to two fence configurations, a Mach number range of 0.60 to 0.89, and one fence location.

UNSTEADY PRESSURE RESULTS - PLAIN CAVITY

Overall root mean square (rms) pressure levels for the plain cavity configurations are presented in Figures 4a and 4b. The data are normalized by the free stream dynamic pressure and represent an averaging over a frequency range from 1 to approximately 50 kHz.

For a free stream Mach number of 0.60 the rms pressure data from the AFFDL test are in good agreement with the Ames data. However, significant differences occur at Mach 0.89 for measurements made inside the cavity and on the flat plate at the cavity leading edge. It is not suggested that such an effect is primarily due to the change in Mach number. In fact, trends in the data for both Mach numbers show that the unsteady pressure levels increase with decreasing local Reynolds number R_ℓ. This decrease with Reynolds number suggests that transitional instabilities in the approaching boundary layer radiate energy which generate more intense fluctuations within the cavity. Since the free stream flow is subsonic, the cavity pressure fluctuations also radiate forward and increase the pressure levels on the plate at the cavity leading edge. Similar findings have been found by previous investigators (Reference 8). They conclude that in comparison to a fully turbulent boundary layer, the laminar portion of a boundary layer "produces more intense fluctuations despite its own lower noise levels".

From the AFFDL and Ames tests it's evident that the scaling of cavity unsteady pressure data should include boundary layer parameters. More experimental work needs to be done before all the important parameters can be defined. However, it appears that transitional effects from the upstream boundary layer can significantly affect the magnitude of cavity resonance.

UNSTEADY PRESSURE RESULTS - CAVITY WITH FENCE

Normalized unsteady pressure data for two fence configurations are presented in Figures 5a and 5b. Comparison of the data along the centerline of the flat plate and cavity floor shows that the AFFDL and Ames tests results are in excellent agreement for both fence configurations. No effect of Reynolds number on cavity resonance or fence effectiveness was found. Both the AFFDL and Ames fences were equally effective in significantly reducing the cavity dynamic pressure levels as compared to the plain cavity. This is probably due to the fact that the fence height h was greater than the local boundary layer thickness δ for both tests. Ratios of $h/\delta_\ell > 1$ were considered to be an important design parameter in order to prevent the shear layer from entering the cavity. Notice that for $h/\delta_\ell = 1.2$, the Ames fence 2 (58% porosity and thus less drag) was equally effective as the Ames fence 1 (38% porosity). Of course, this neglects the differences in free stream Mach number.

UNSTEADY PRESSURE SPECTRA RESULTS - PLAN CAVITY AND CAVITY WITH FENCE

Nondimensional resonant frequency data or Strouhal numbers ($S = fd/V_\infty$) for both the Ames and AFFDL cavity tests are presented as a function of free stream Mach number in Figures 6a and 6b. Frequency data from the Ames test were obtained from a varying bandwidth analysis between 2 and 800 Hz. The AFFDL data were obtained from a narrow bandwidth analysis with

a frequency resolution of $\pm$ 20 Hz. The solid curves represent calculated values of Strouhal number for various cavity resonance modes m. These curves were calculated from the following modified Rossiter equation obtained from Reference 1:

$$m = 1,2,3,4$$

$$S = \frac{m - 0.25}{\frac{M}{\left[1 + \frac{k-1}{2} M^2\right]^{\frac{1}{2}}} + 1.75}$$

where M is the free stream Mach number and k is the ratio of specific heats.

For the first fundamental mode and the second harmonic both the Ames and AFFDL frequency data are in excellent agreement for the plain cavity case (Figure 6a). In addition, predicted values using the Rossiter equation are in good agreement with the measured data, especially for the first mode. Significant differences are found between the two tests and also between the test and predicted values for m = 4. The differences between the experimental data are probably due to the relatively large bandwidth of the Ames data at the higher frequencies. In any case, the lower resonant modes have the highest energy content and thus are of greater importance.

Comparison of the AFFDL and Ames data for the cavity with fence configuration are shown in Figure 6b. Excellent agreement between experiments and predicted values were also obtained with results similar to the plain cavity case. It's interesting to note that, although the fences significantly reduce the cavity dynamic pressures, the same resonant

frequencies are still present but at a much lower energy level. Consequently the Rossiter equation, although not developed for the cavity with fence configuration, still successfully predicts the cavity resonant frequencies.

SECTION IV

TURRET/FAIRING TESTS

MODELS AND TEST FACILITIES

In this section, selected data from several wind tunnel and flight tests are compared. The drag data presented were obtained from experiments conducted in the Air Force Academy (AFA) and AFFDL transonic wind tunnels. Two separate 0.025 scale models of a turret with a high rise aft fairing were mounted in the wind tunnels on a hollow circular cylinder with forward and aft ramps. The cylindrical section was designed to approximate the upper forward portion of a KC-135 aircraft fuselage. A sketch of the model configuration is shown along with the drag data in Figure 7.

The unsteady pressure data presented in this section were obtained from experiments conducted in the AFFDL 0.61 m by 0.61 m (2 ft by 2 ft) and NASA-Ames 4.27 m by 4.27 m (14 ft by 14 ft) wind tunnels and from flight tests of the Airborne Laser Laboratory (ALL). The wind tunnel models were candidate configurations of the ALL cycle III/IV aft fairing with a forward ramp. A configuration sketch is shown in Figure 8. The AFFDL and NASA-Ames model scales were 0.025 and 0.30 respectively.

TYPES OF MEASUREMENTS AND TEST CONDITIONS

Data recorded during the AFA and AFFDL high rise fairing/turret tests included force measurements and oil flow visualization photography. Only the drag force data are presented in this paper for a Mach number range from 0.60 to Mach 0.90. At the AFA, the free stream unit Reynolds number varied with tunnel Mach number while at AFFDL, the free stream unit Reynolds number was a constant. The drag data ΔC_D which is presented in Figure 7 reflects drag caused by the addition of the turret

and fairing only and are based upon the forward projected area of the turret (Ref. 9). The Reynolds numbers R_D are based on the turret diameter D.

Selected unsteady pressure data from the AFFDL and NASA-Ames wind tunnels and the ALL flight tests are presented in this paper. The locations of the dynamic pressure transducers on the turret, forward ramp, and aft fairings are shown in Figure 8. Data results from these tests are presented in Figures 9a through 9d for a Mach number range from 0.50 to Mach 0.90. Turret Reynolds numbers varied from $R_D = 2.3 \times 10^5$ to $R_D = 40 \times 10^5$.

Two nondimensional power spectal density plots are also shown in Figures 10a and 10b comparing the 0.30 scale and full scale tests at Mach numbers of 0.55 and 0.75. However, these data were obtained from tests of a different fairing than that shown in Figure 8. They are presented here because they were the only wind tunnel and flight test data available and show that both power spectra data as well as root mean square pressure data can be correlated.

DRAG DATA RESULTS - AFA AND AFFDL TESTS

Several important observations can be made from the drag data results presented in Figure 7. Consider the drag versus Mach number curve for the bare turret configuration. If the two tests were dynamically similar, one would expect these curves to show much better agreement. As expected, the higher drag curve is at the lower turret Reynolds number. Differences between the two curve shapes is probably due to the variation of Reynolds number with free stream Mach number. Similar Reynolds number effects are also observed for the turret and aft fairing configuration. However, the two curve shapes are in much better agreement.

Although dynamic similarity between these two tests was incomplete, some very useful and important results exist which should not be overlooked. First, both configurations for both tests indicate an increase in drag with increasing Mach number. This, of course, was to be expected since similar results have been measured for flow around spheres and can be attributed to the appearance of unstable shock waves. A more important result, however, is found in the ranking of the drag curves. Both tests show the fairing drag to be less than the bare turret drag and for both configurations the AFA data ranks lower than the AFFDL data. The important point to be made here is that such trends in the data are useful results. Although the absolute drag coefficients cannot be compared between each test, both tests can be used to provide useful information concerning the effectiveness of one configuration over another.

UNSTEADY PRESSURE RESULTS - AFFDL, AMES, AND FLIGHT TESTS

Generally speaking, the unsteady pressure data presented in Figures 9 and 10 show good correlation between the AFFDL and NASA-Ames wind tunnel tests and the ALL flight tests. The best correlations are found in Figures 9c and 9d and in Figures 10a and 10b. First, it should be noted that the instrumentation locations for each test were substantially different in some cases. Consequently, the data comparisons would be expected to be poor especially in highly unstable flow regions. Figure 9a is such a case. Not only are the pressure transducers at very different locations but they are also located in a very turbulent flow region on the turret and aft fairing. At these locations local shock waves form, the flow separates from the turret and then reattaches to the fairing. Better agreement between tests is shown in Figure 9b although there are some discrepancies with the flight test data at the

lower Mach numbers. The reason for this is not clear, but is possibly due to a local separated flow region on the ALL fairing. The best agreement, of course, is shown in Figures 9c and 9d where the flow is attached and fairly stable. Notice that for these locations the unsteady pressure levels are much lower than those of Figures 9a and 9b. Since the flow is attached in these areas, the measurement is primarily due to boundary layer noise. Other differences between transducers such as those in Figures 9c and 9d are most likely attributed to differences in spatial resolution of the instrumentation between tests.

All in all, the unsteady pressure data show good correlation and provide a fairly accurate picture of the flow phenomena which occurs at different locations. As was the case with the drag data discussed earlier, the unsteady pressure data from each test also show similar trends. In the highly unstable regions (Figures 9a and 9b) all three tests show a decrease in the unsteady pressure levels with an increase in the free stream Mach number. In the stable flow regions (Figures 9c and 9d) all three tests show very little change in the unsteady pressure levels with Mach number.

Finally, when comparing flight and wind tunnel power spectral density data excellent correlations have been obtained (see Figures 10a and 10b). However, it should be emphasized that these data were obtained from tests of a much different configuration than the cycle III/IV configuration shown in Figure 8. The pressure transducers were at the top of the turret (same as location A in Figure 8) but were in a very protected region behind a high rise forward ramp fairing.

SECTION V

CONCLUSIONS

Data from several wind tunnel experiments along with available flight test data were used to discuss the validity of small scale tests. Tests were performed at transonic speeds to measure the turbulence levels in a cavity with and without a forward porous fence, turret drag with and without an aerodynamic fairing, and turret/fairing unsteady pressures. Analysis of the test results leads to the following conclusions:

1. Porous fences were found to be effective in reducing cavity unsteady pressure levels of small scale models. However, scaling the magnitude of unsteady pressure reduction to full scale is uncertain. The data shows that there is a fixed ratio of fence height to cavity length independent of model scale.

2. Trends and levels of unsteady pressure coefficients on turrets and fairings are predicted by small scale tests in regions of attached flow. In regions susceptible to flow separation such as on the turret itself, small scale data are not expected to scale up because of Reynolds number effects.

3. Resonant frequencies of a plain cavity and a cavity with a porous fence can be predicted for small scale tests.

4. Upstream boundary layer conditions can significantly influence the degree of correlation between different small scale cavity tests.

REFERENCES

1. Conner, W. R., Airborne Laser Laboratory Exhaust Channel Acoustic Analysis, AFFDL-TR-75-149, February 1976.

2. McDermott, D. J., Airborne Laser Laboratory Cavity and Fence Tests, AFFDL-TR to be published.

3. Buell, D. A., Aerodynamic Properties of a Flat Plate with Cavity for Optical Propagation, NASA TM 78487, January 1979.

4. Van Kuren, J. T. and Conner W. R., Fairing Design For Fuselage Mounted Turret in Transonic Flow, AFFDL-TM-73-115 FXM, September 1973.

5. Van Kuren, J. T., Walterick R. E. and McDermott, D. J., Transducer Sensitivities For Unsteady Pressure in Transonic Flow, 46th Semi-Annual Supersonic Wind Tunnel Association Meeting, October 1976.

6. Walterick R. E. and Van Kuren, J. T., Wind Tunnel Tests Of Fairings For An On-Gimbal Telescope Turret, AFFDL-TM-75-177 FXM, November 1975.

7. Van Kuren, J. T., Experiments to Develop a Thick Turbulent Boundary Layer For Optical Degradation Measurements, AFFDL-TM-75-106-FX, June 1975.

8. Heller, H. H., Holmes, D. H. and Covert E. E., Flow Induced Pressure Oscillations in Shallow Cavities, 1971 Journal of Sound and Vibration 18, pp. 565-553.

9. Shapiro, A, H., Shape and Flow - The Fluid Dynamics of Drag, 1961.

FENCE CONFIGURATIONS

TABLE 1

FENCE #	HEIGHT	WIDTH	THICKNESS	% POROSITY	REMARKS
1	0.89 cm (AFFDL) 2.29 cm (AMES)	25.40 cm	0.51 cm	38	A) ONE ROW OF HOLES 0.52 cm IN DIAMETER. FORTY-THREE HOLES PER ROW. (THREE ROWS AND 35 HOLES PER ROW FOR AMES FENCE) B) FENCE LOCATED 4.06 cm UPSTREAM OF CAVITY LEADING EDGE
2	2.29 cm (AFFDL & AMES)	25.40 cm	0.51 cm	58	A) TWO ROWS OF HOLES 0.99 cm IN DIAMETER. TWENTY-TWO HOLES PER ROW. B) FENCE LOCATED 4.06 cm UPSTREAM OF CAVITY LEADING EDGE

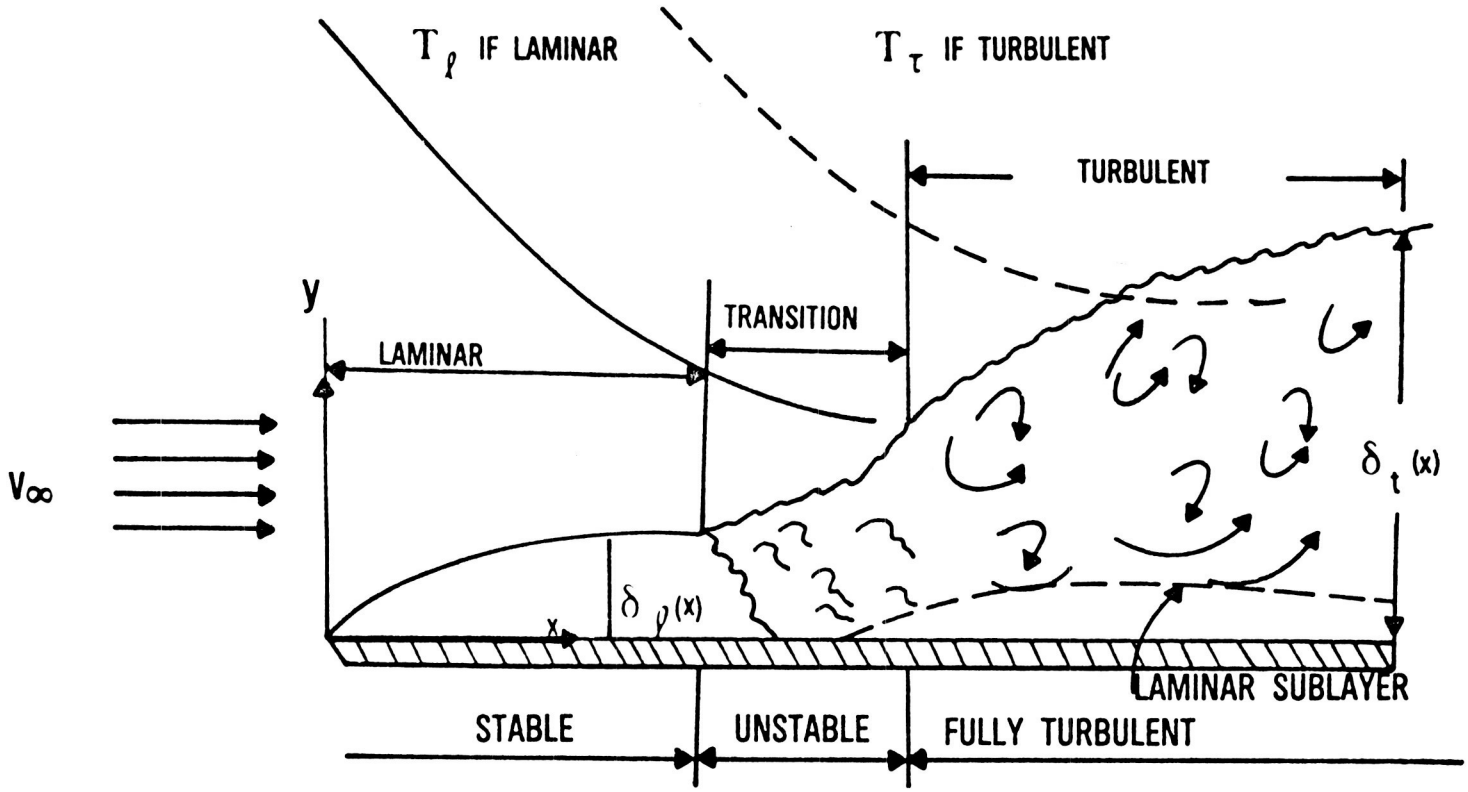

FIGURE 1

DEVELOPMENT OF A BOUNDARY LAYER ON A FLAT PLATE.

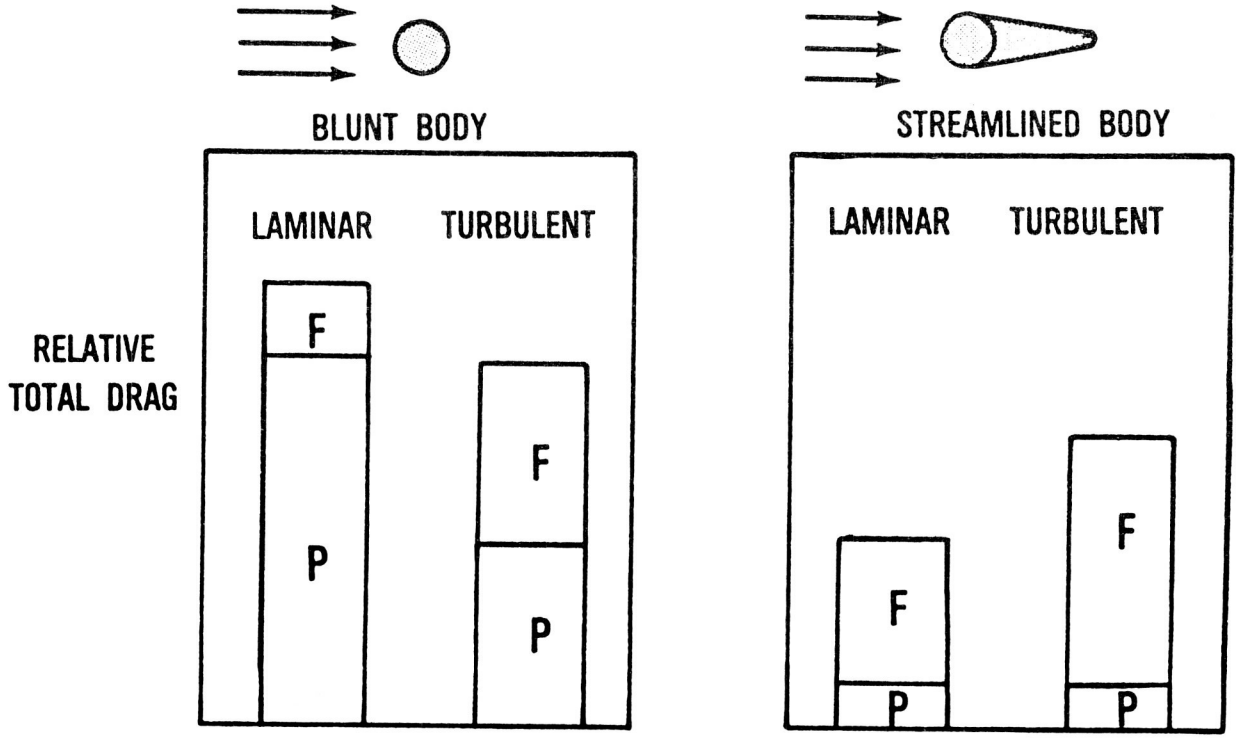

FIGURE 2

THE RELATIVE EFFECTS OF FRICTION AND PRESSURE DRAG IN LAMINAR AND TURBULENT FLOWS FOR BLUNT AND STREAMLINED BODIES.

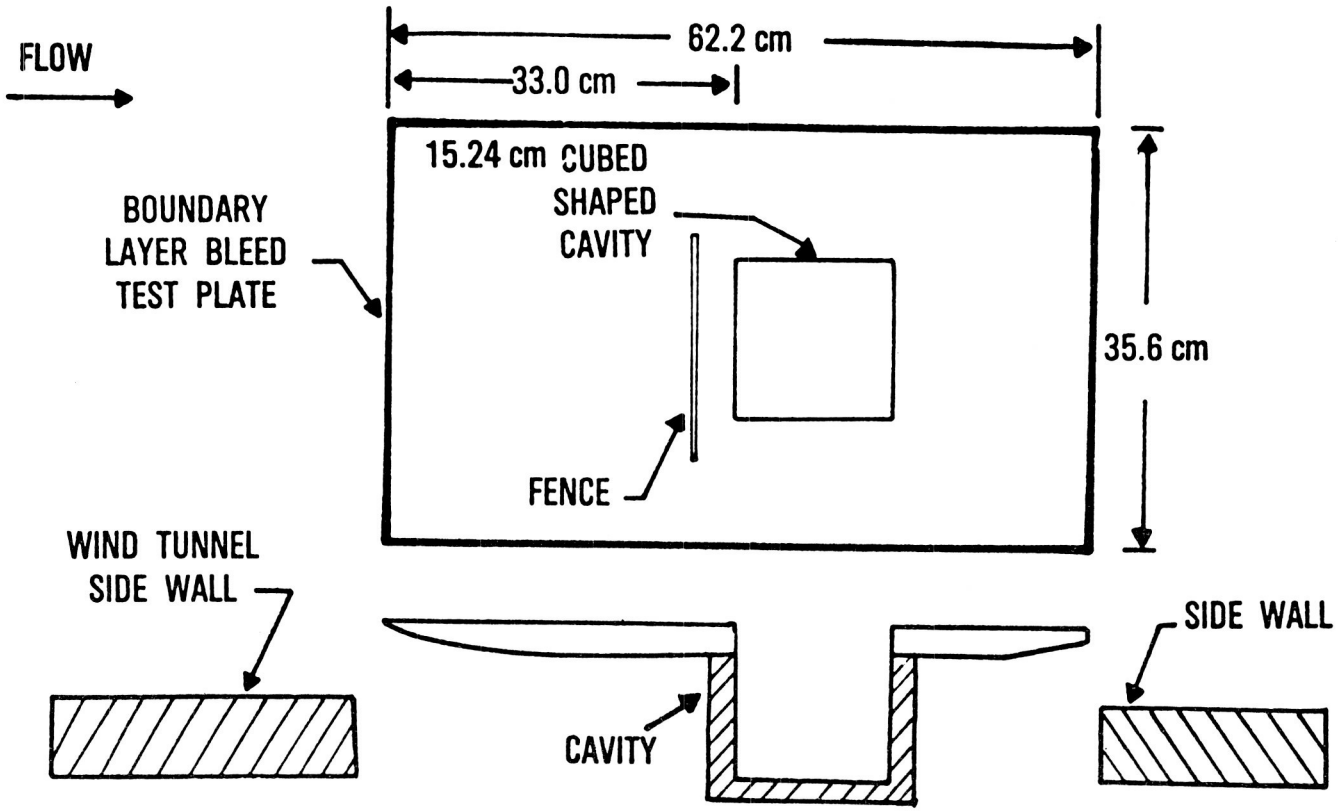

FIGURE 3a

AFFDL FLAT PLATE MODEL WITH CAVITY.

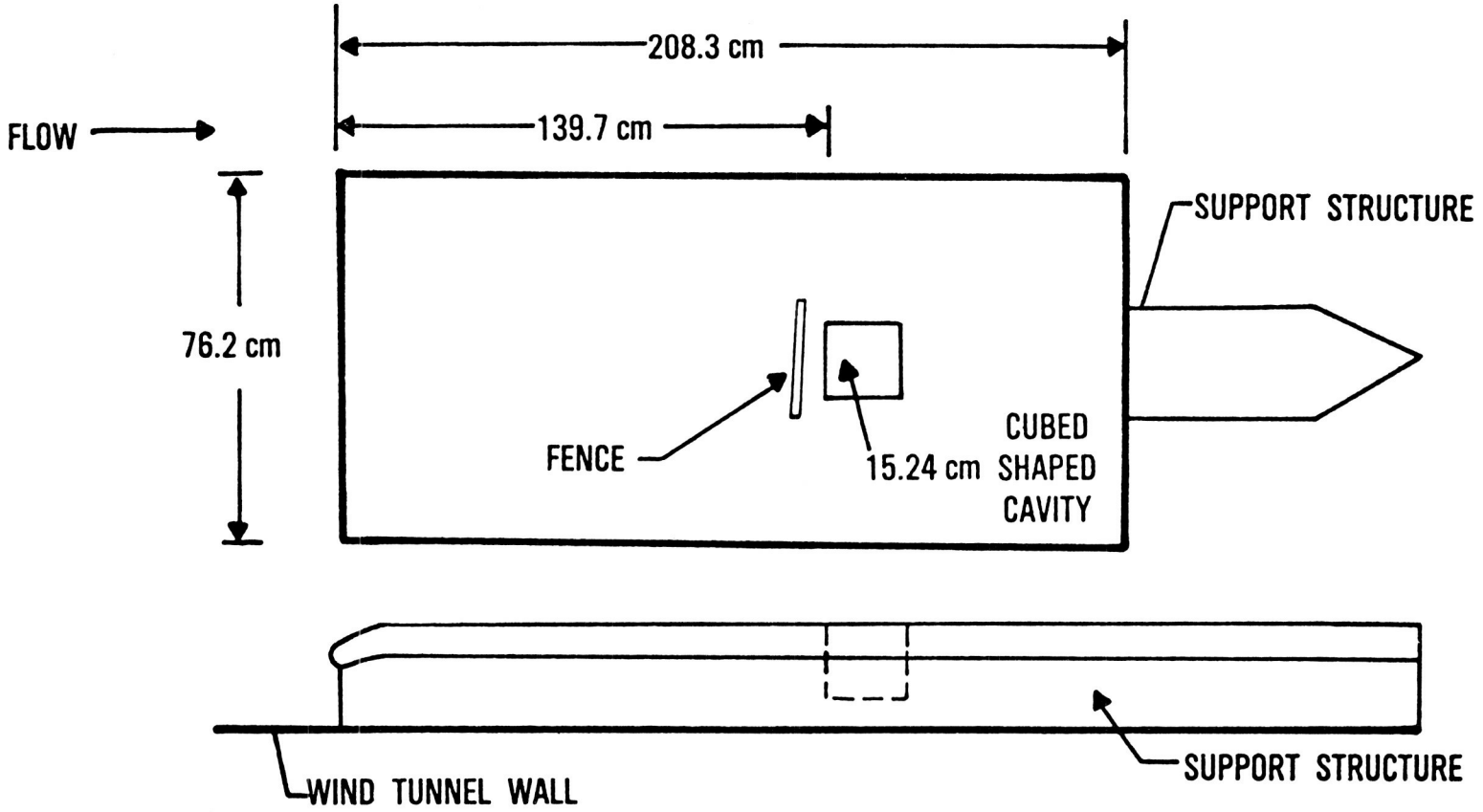

FIGURE 3b
NASA – AMES FLAT PLATE MODEL WITH CAVITY.

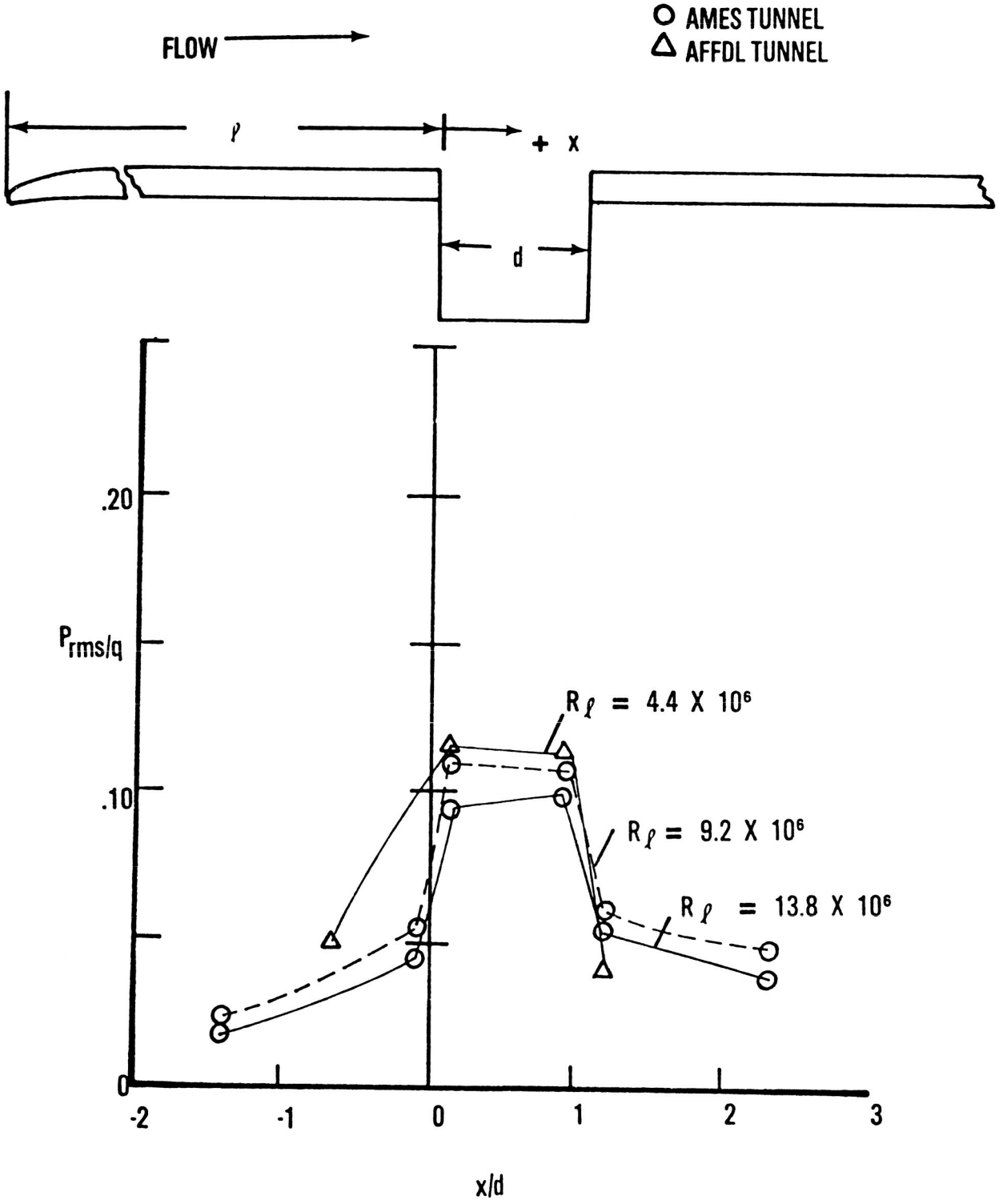

FIGURE 4a

COMPARISON OF NASA-AMES AND AFFDL DYNAMIC PRESSURE DATA ALONG THE CENTERLINE OF THE FLAT PLATE AND CAVITY FLOOR. PLAIN CAVITY, M = 0.60.

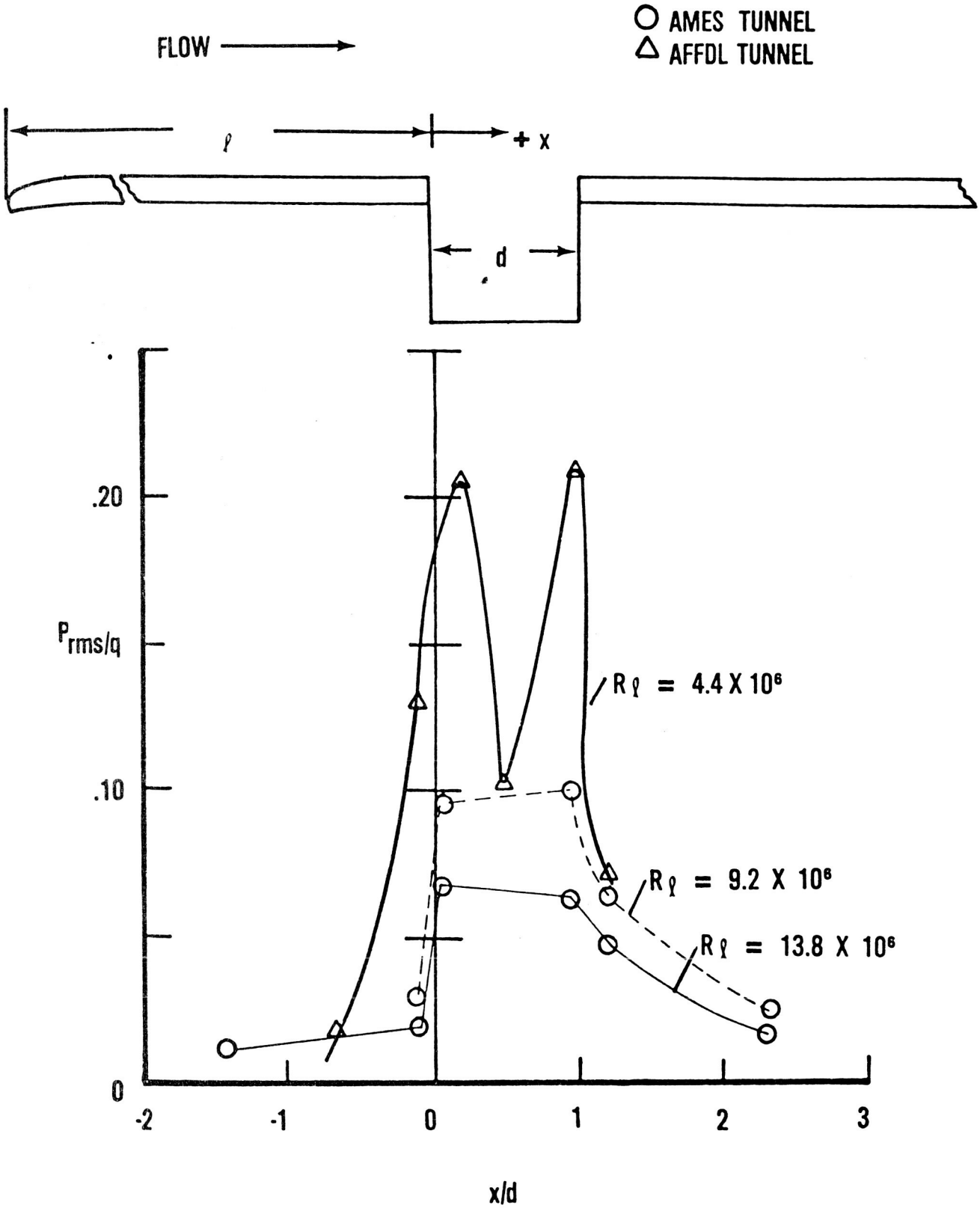

FIGURE 4b

COMPARISON OF NASA–AMES AND AFFDL DYNAMIC PRESSURE DATA ALONG THE CENTERLINE OF THE FLAT PLATE AND CAVITY FLOOR. PLAIN CAVITY, M = 0.89.

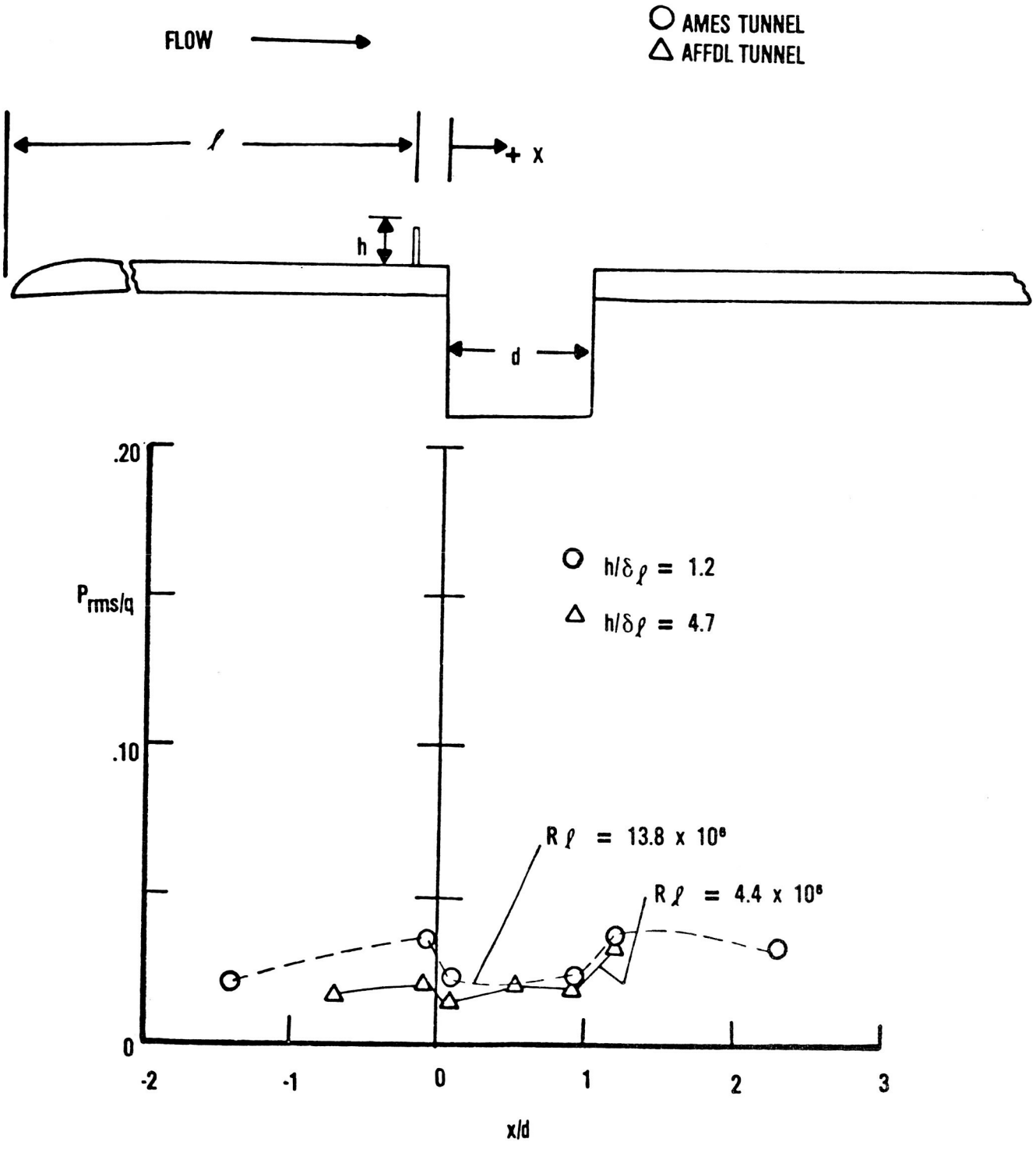

FIGURE 5a

COMPARISON OF NASA-AMES AND AFFDL DYNAMIC PRESSURE DATA ALONG THE CENTERLINE OF THE FLAT PLATE AND CAVITY FLOOR. CAVITY WITH FENCE 1, M = 0.60.

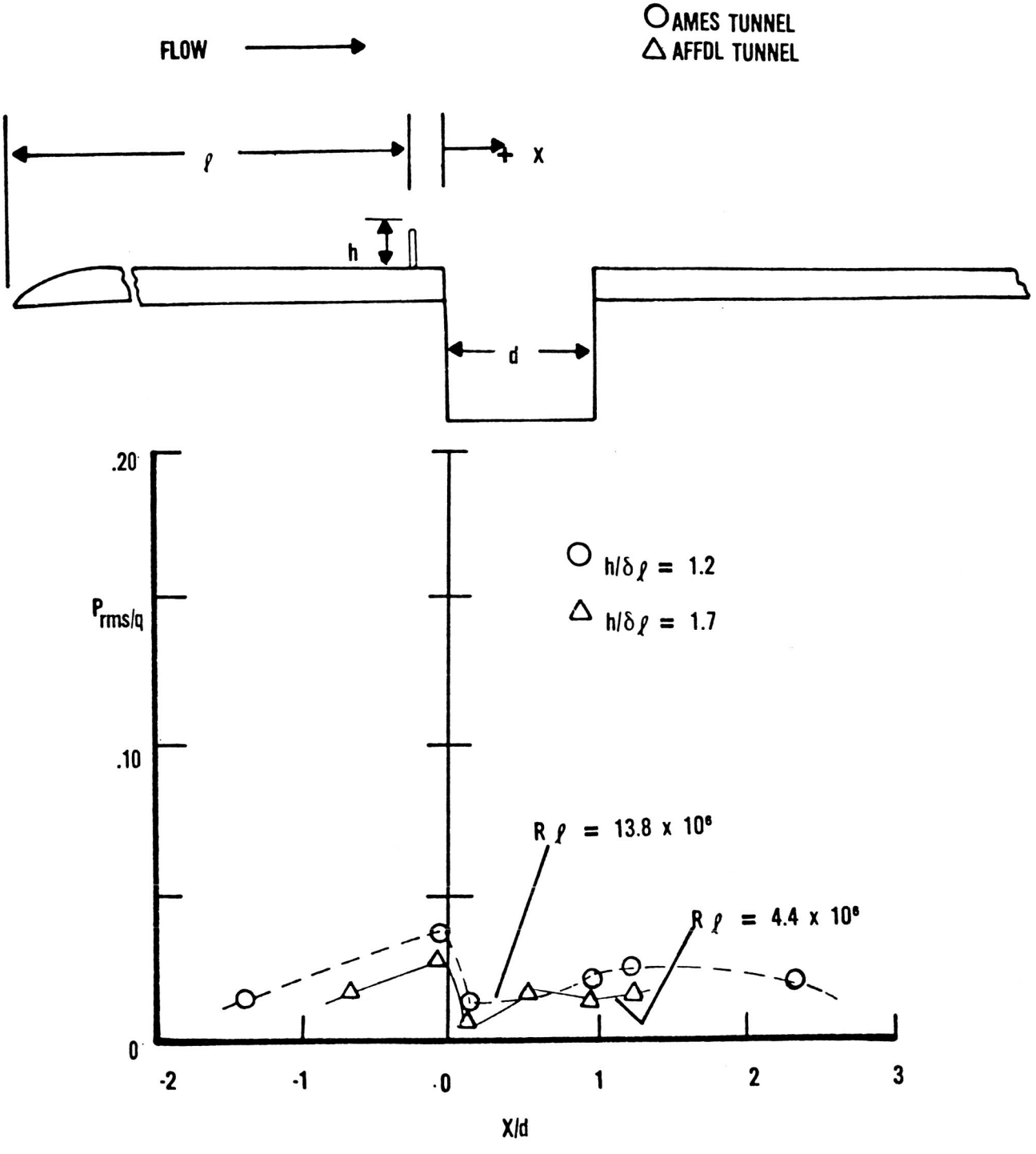

FIGURE 5b

COMPARISON OF NASA–AMES AND AFFDL DYNAMIC PRESSURE DATA ALONG THE CENTERLINE OF THE FLAT PLATE AND CAVITY FLOOR. CAVITY WITH FENCE 2, M = 0.89.

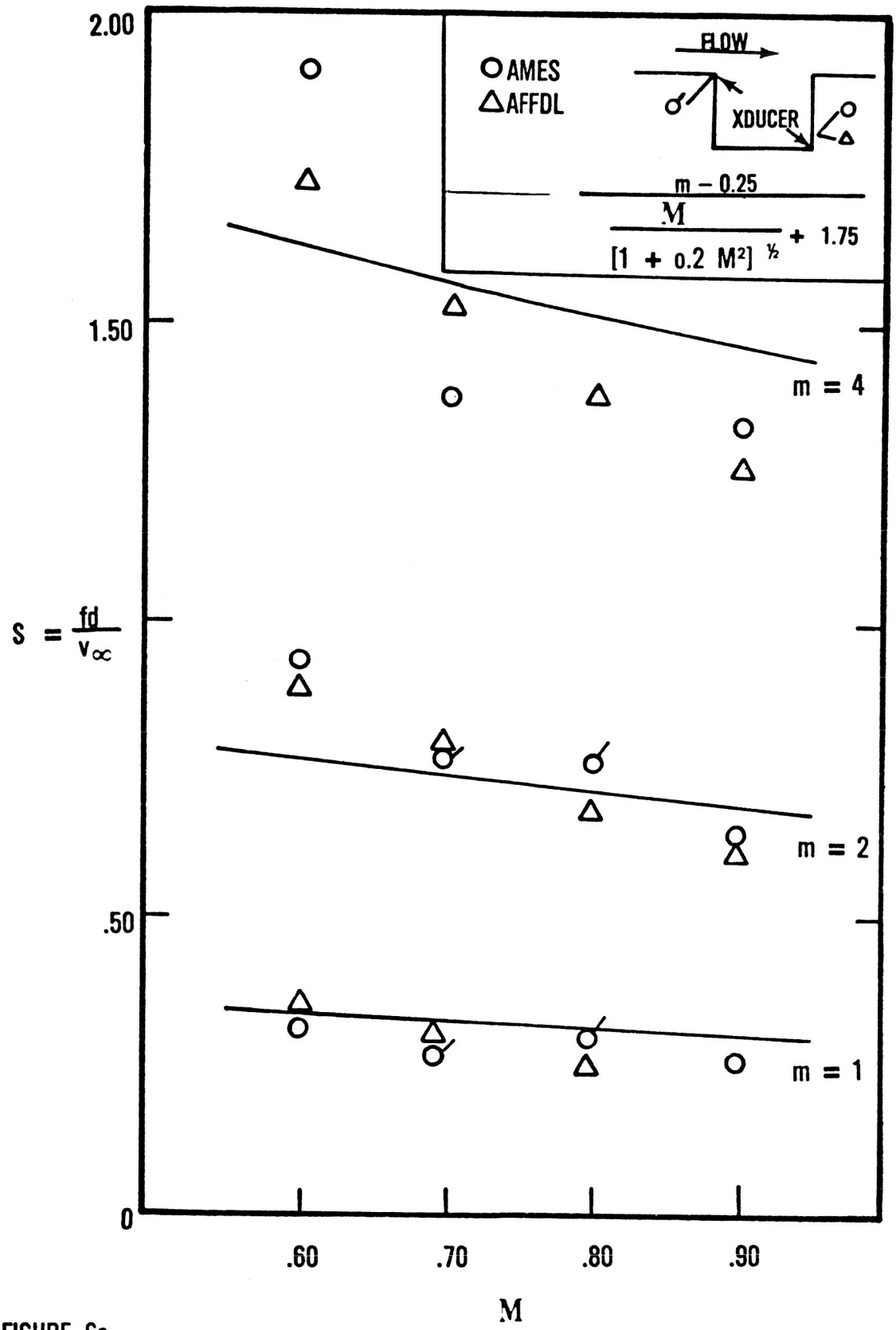

FIGURE 6a

COMPARISON OF NASA–AMES AND AFFDL NONDIMENSIONAL RESONANT FREQUENCY DATA AS A FUNCTION OF MACH NUMBER. PLAIN CAVITY.

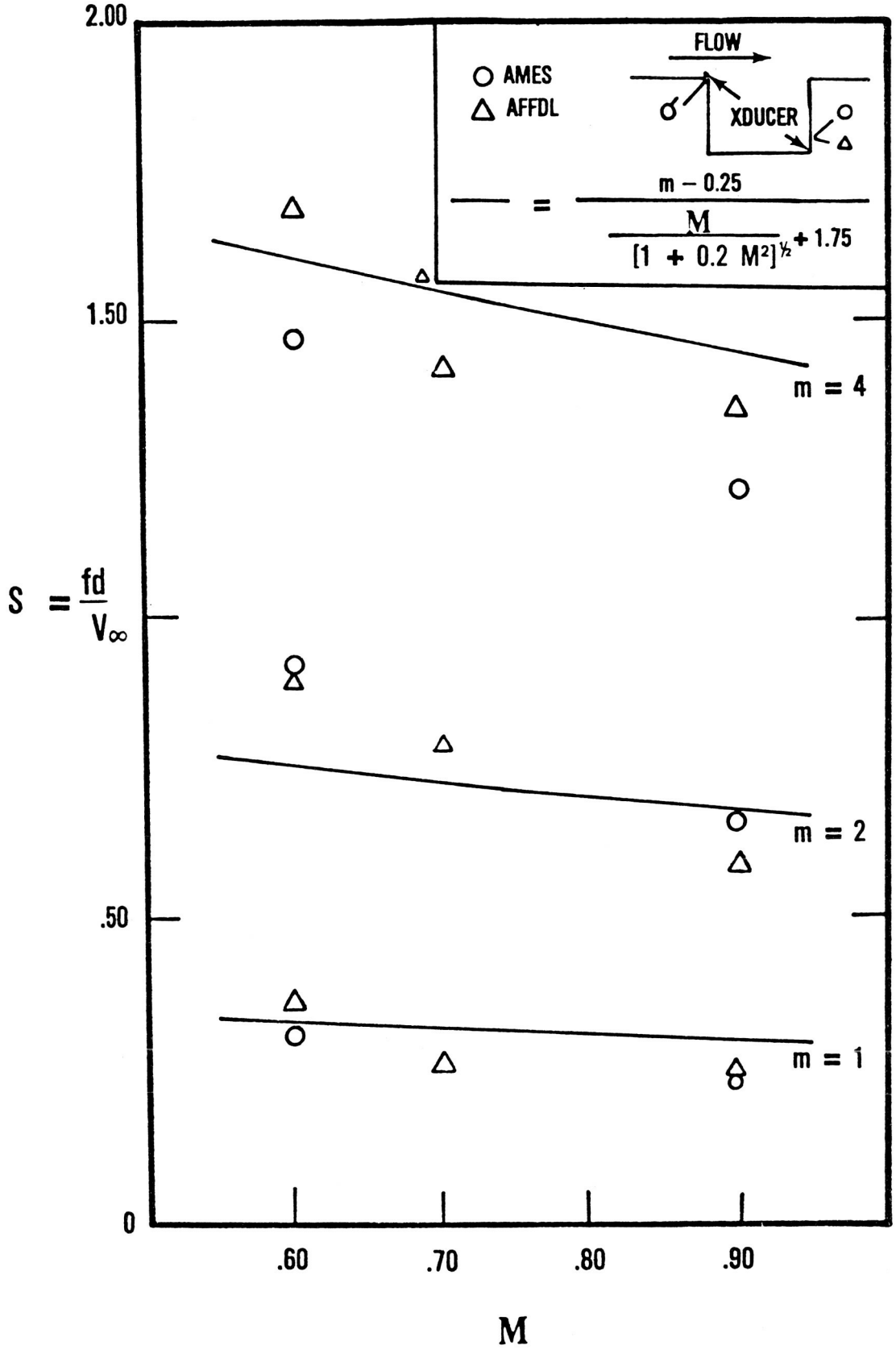

FIGURE 6b

COMPARISON OF NASA–AMES AND AFFDL NONDIMENSIONAL RESONANT FREQUENCY DATA AS A FUNCTION OF MACH NUMBER. CAVITY WITH FENCE 2.

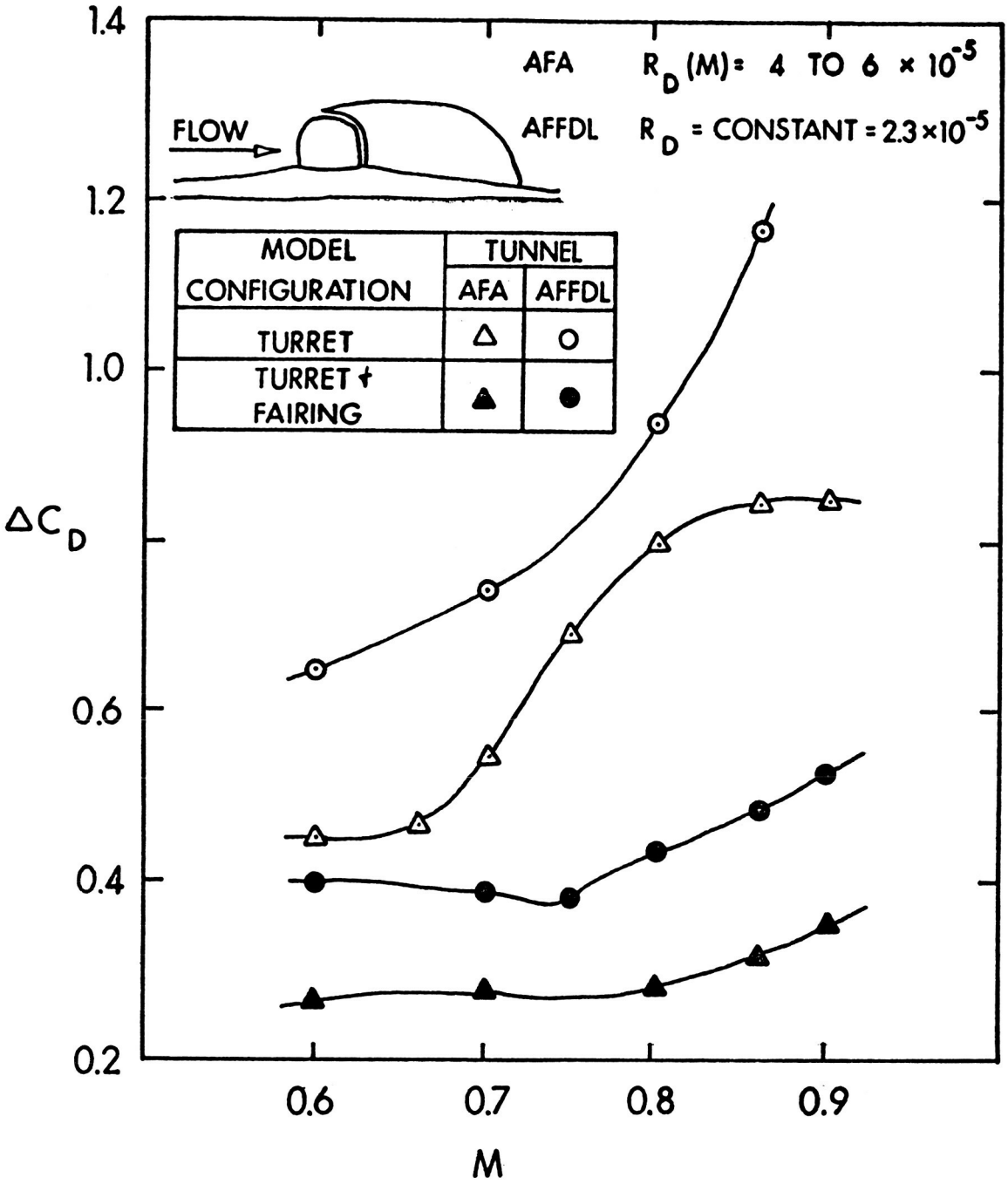

Figure 7

COMPARISON OF AIR FORCE ACADEMY AND AFFDL FAIRING AND TURRET DRAG DATA AS A FUNCTION OF MACH NUMBER.

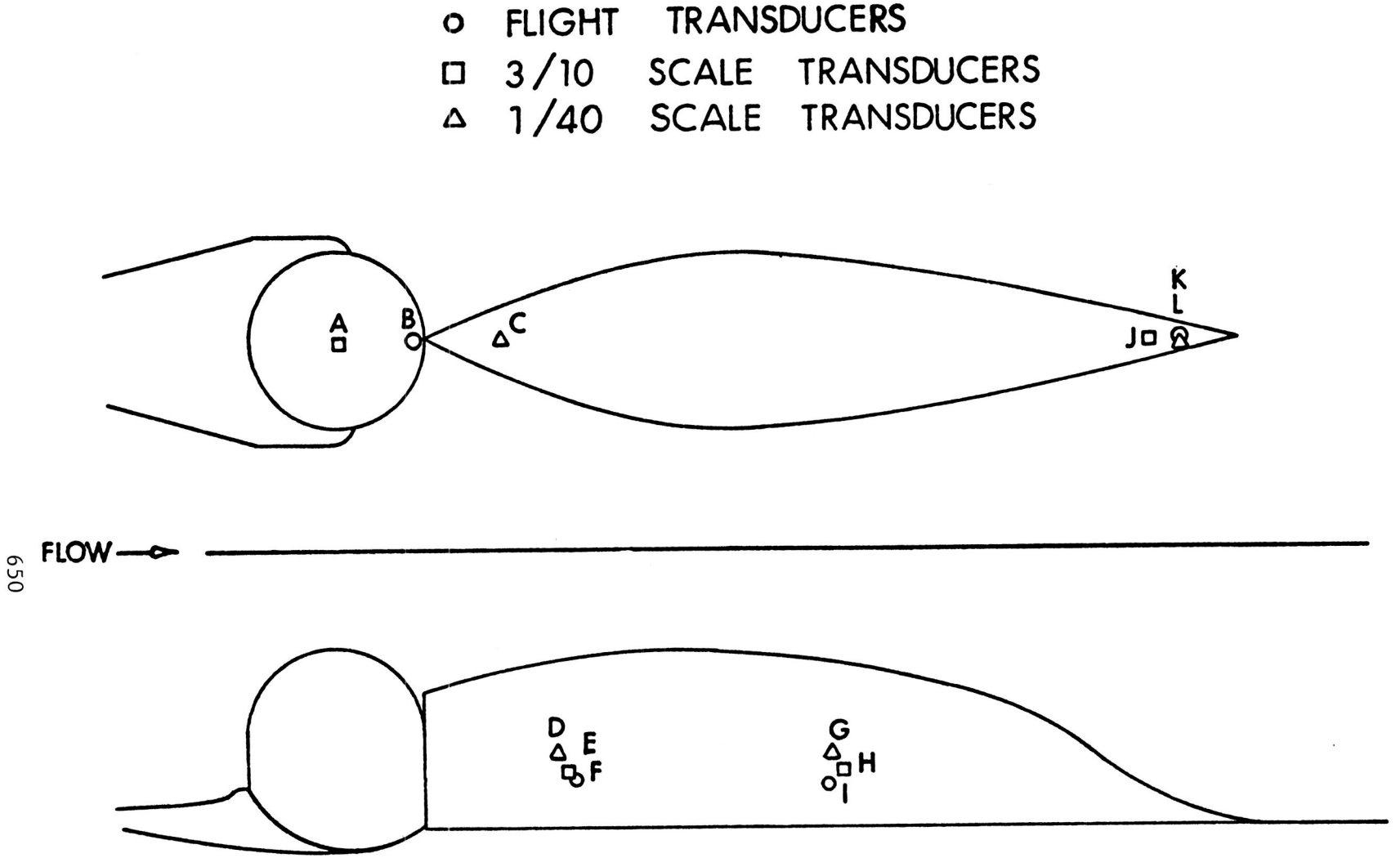

Figure 8 PRESSURE TRANSDUCER LOCATIONS ON ALL CYCLE III/IV TURRET AND FAIRING.

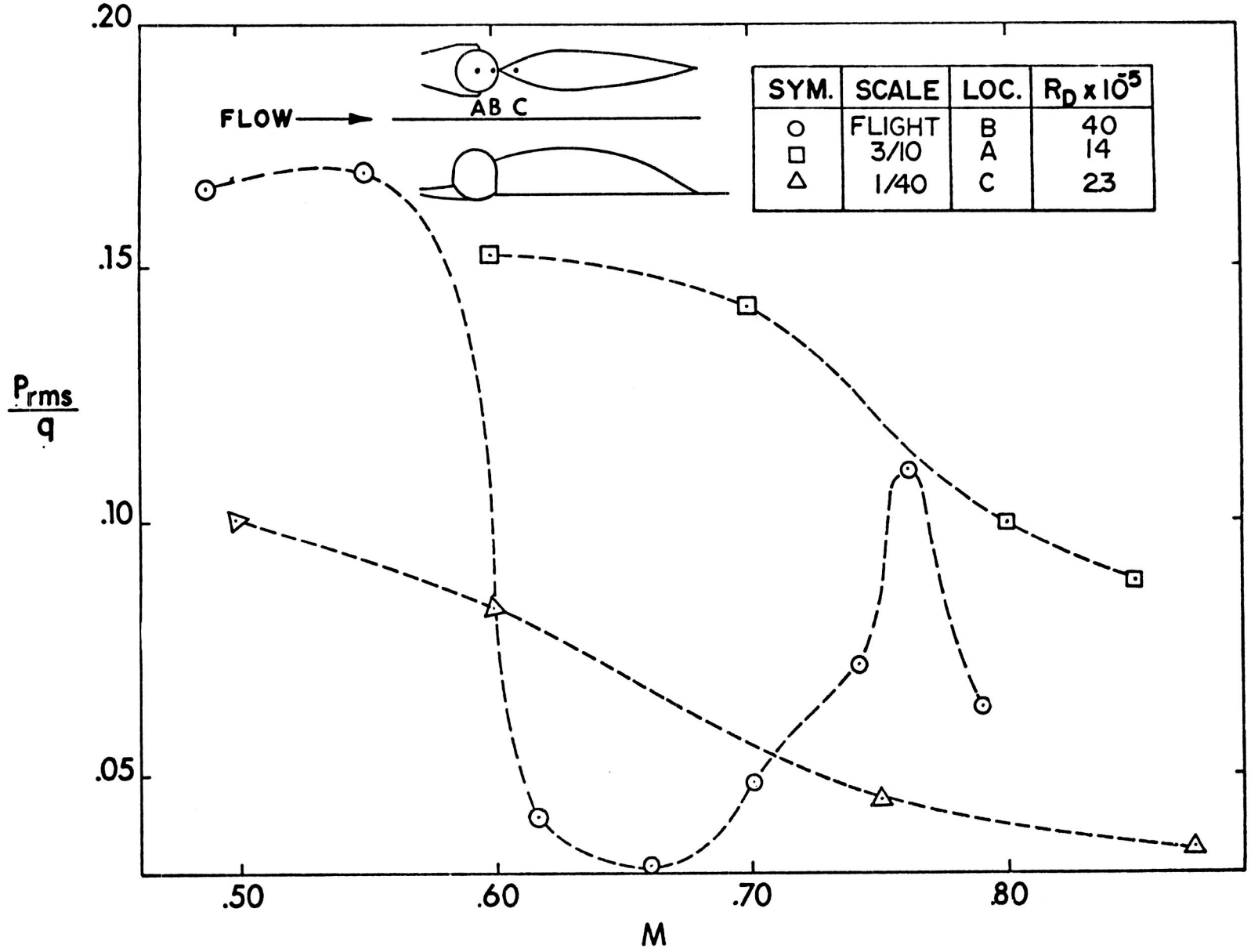

Figure 9a : COMPARISON OF THE CYCLE III/IV TURRET-FAIRING DYNAMIC PRESSURE DATA FROM AFFDL AND NASA AMES WIND TUNNEL AND ALL FLIGHT TEST. PRESSURE.

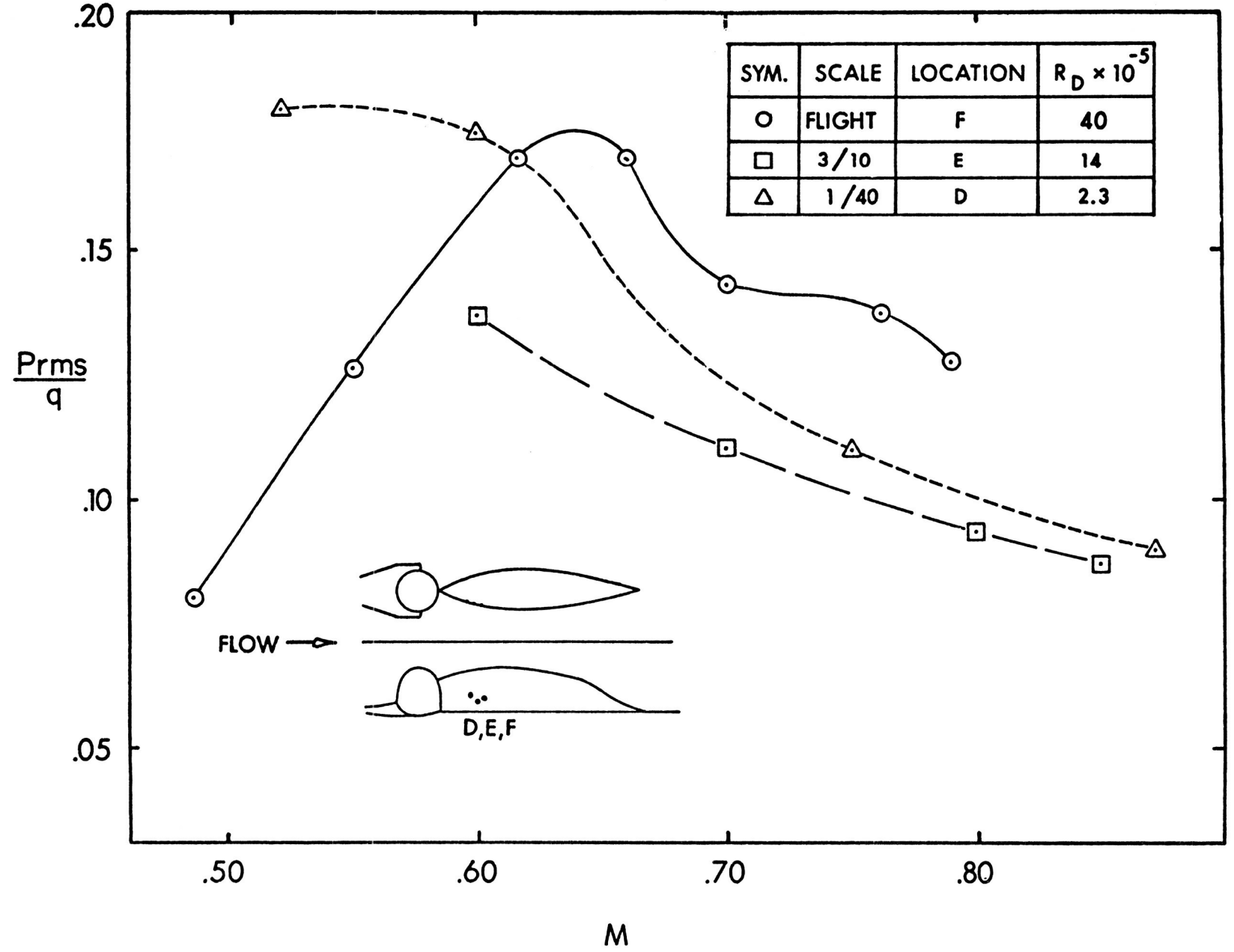

Figure 9b PRESSURE TRANSDUCER AT D,E, AND F, LOCATIONS.

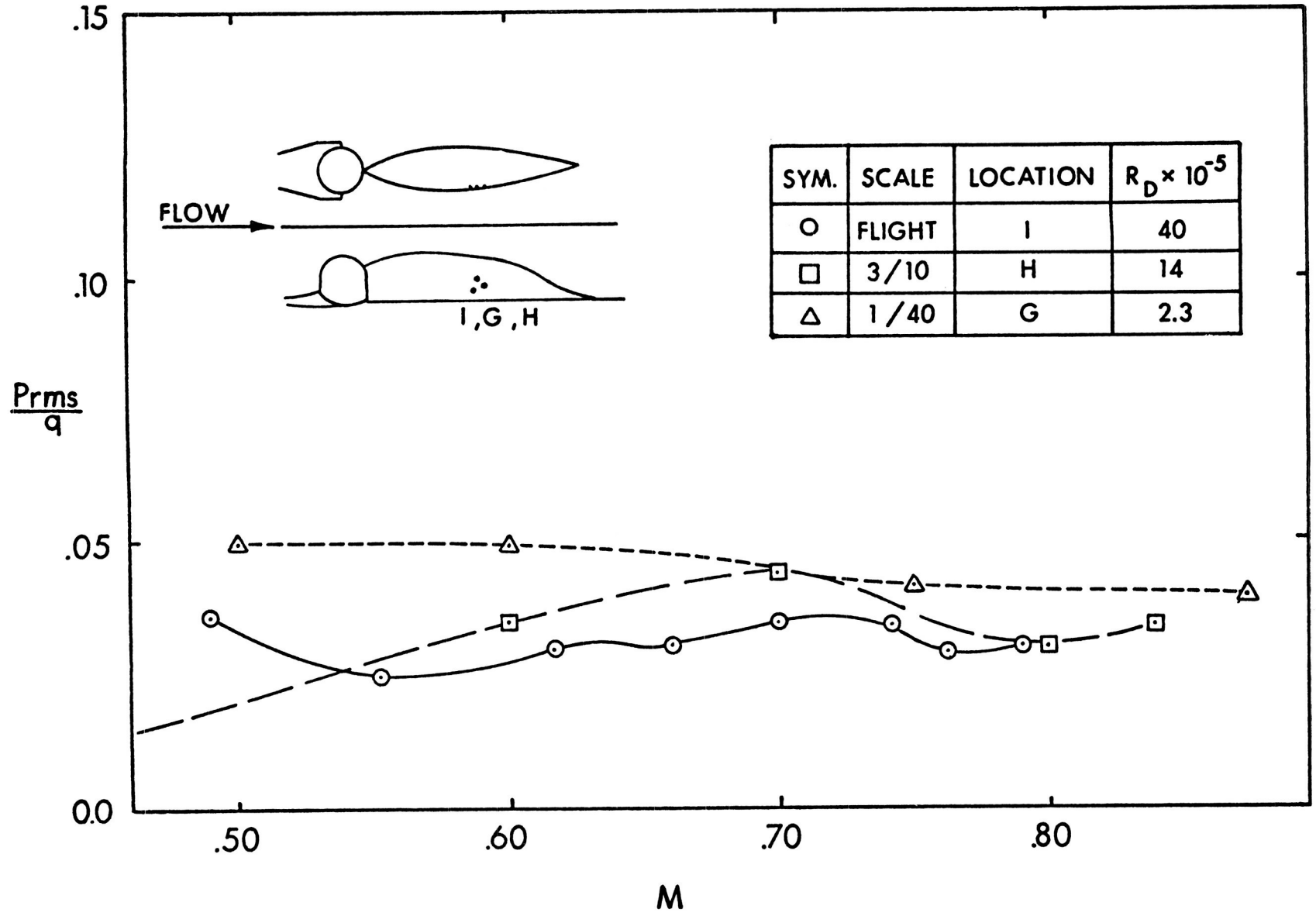

Figure 9c PRESSURE TRANSDUCER AT I,H, AND G LOCATIONS.

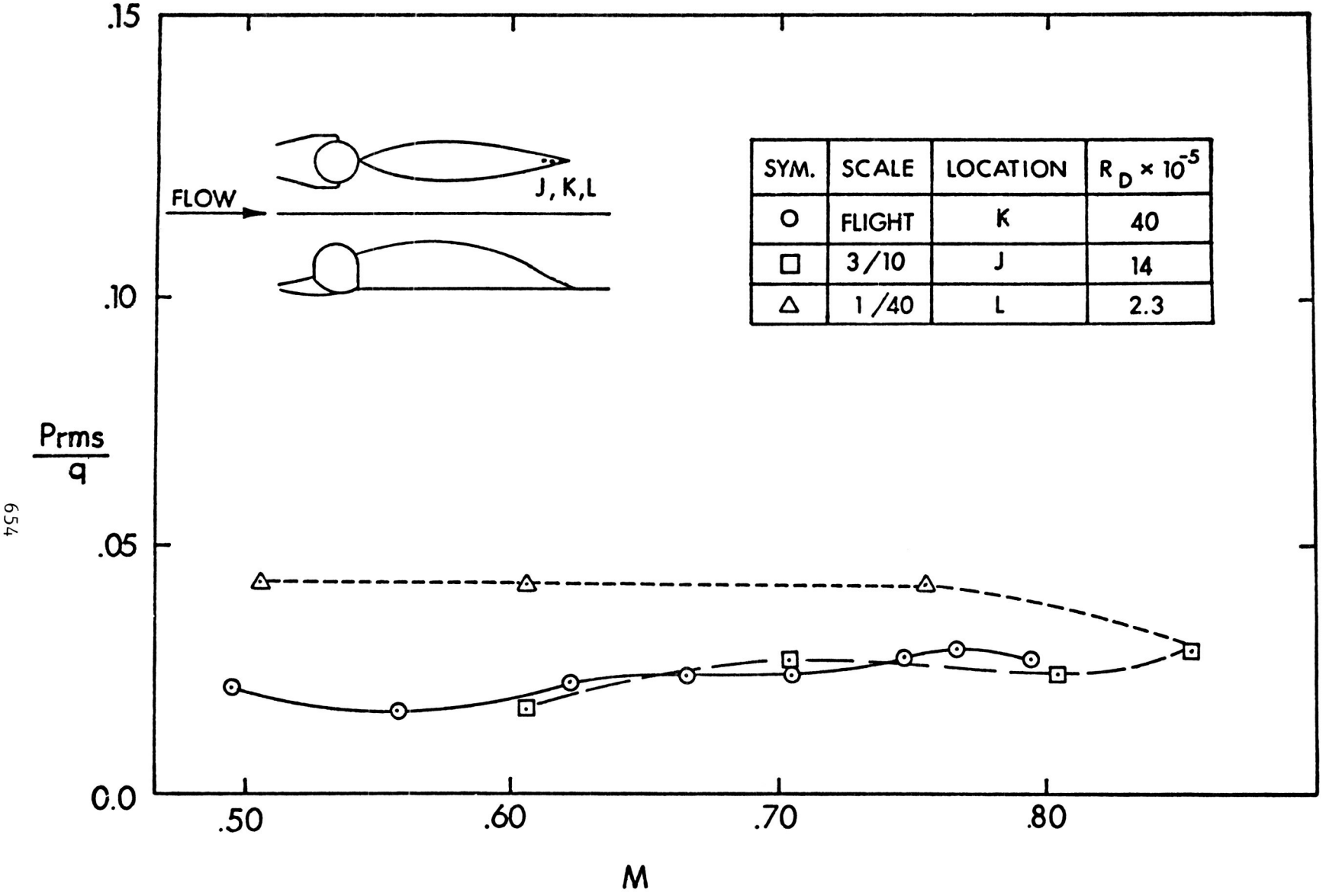

Figure 9d PRESSURE TRANSDUCER AT K, J, AND L LOCATIONS

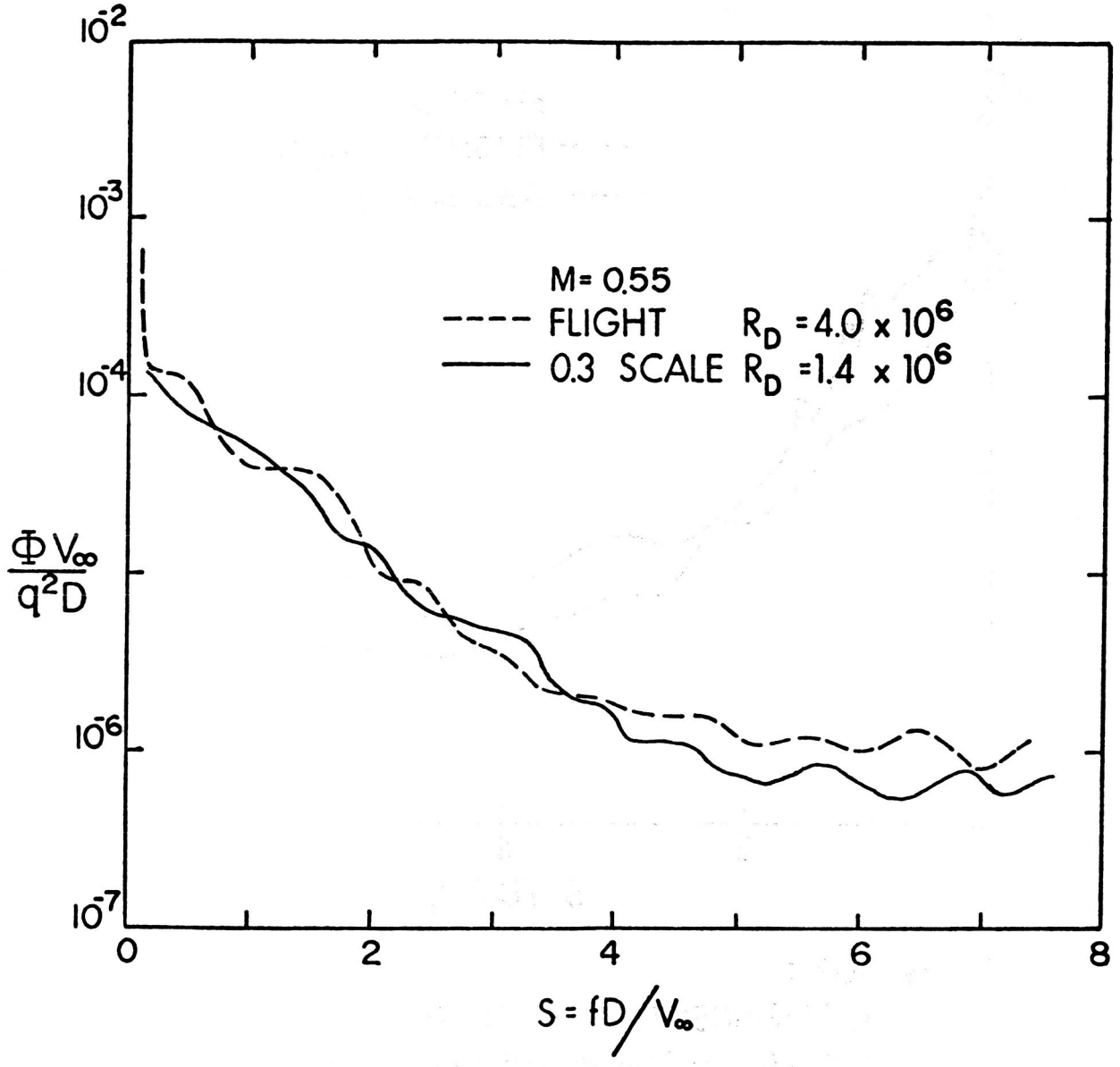

Figure 10a:
COMPARISON OF FLIGHT AND AMES 0.30 SCALE NONDIMENSIONAL POWER SPECTRAL DENSITIES. TRANSDUCERS ON TOP OF TURRET, M=0.55.

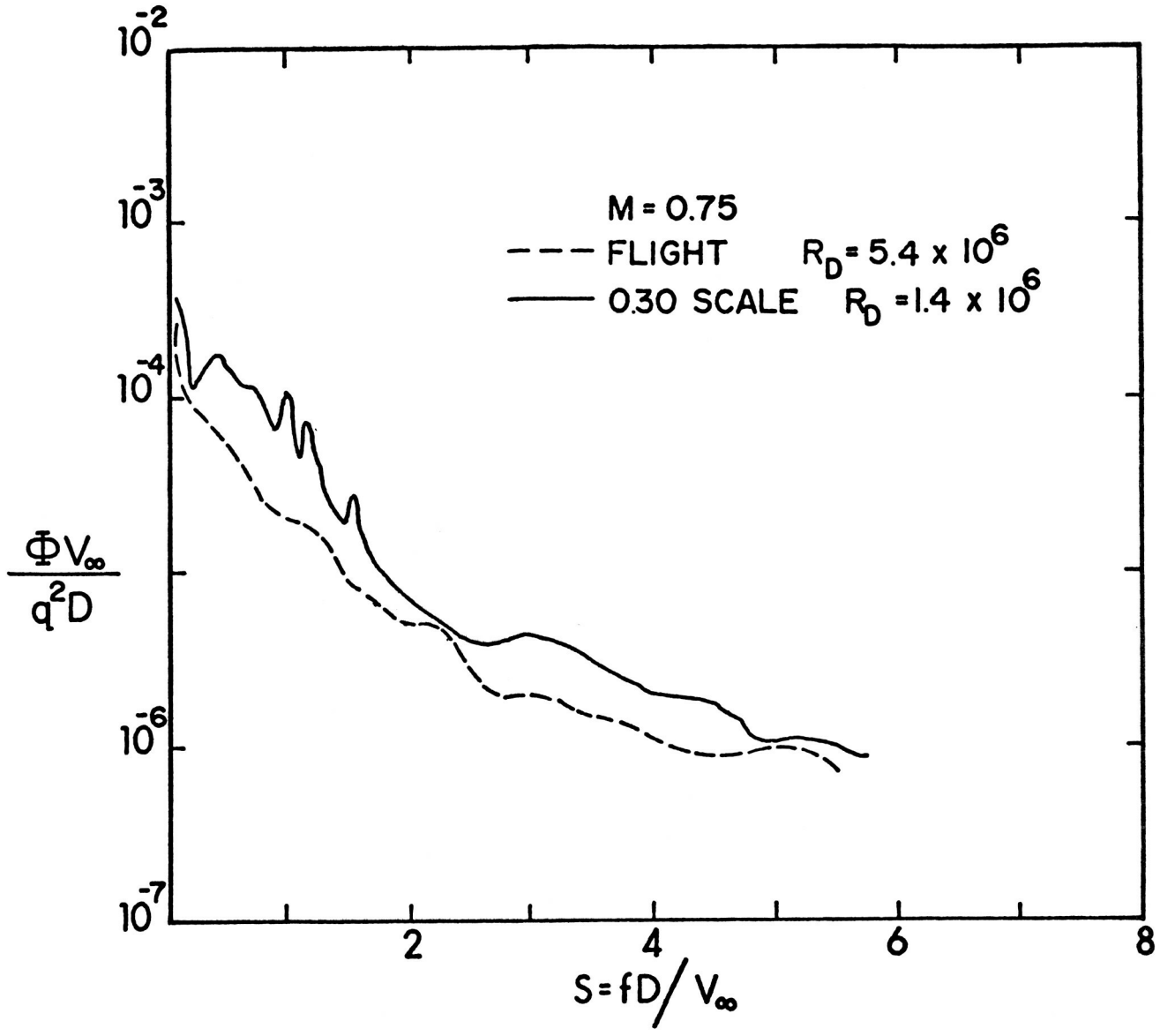

Figure 10b :
COMPARISON OF FLIGHT AND AMES 0.30 SCALE NONDIMENSIONAL POWER SPECTRAL DENSITIES. TRANSDUCER ON TOP OF TURRET, M = 0.75.